

Estimating Eigenenergies from Quantum Dynamics: A Unified Noise-Resilient Measurement-Driven Approach

Yizhi Shen,^{1,*} Daan Camps,² Aaron Szasz,¹ Siva Darbha,^{1,2} Katherine Klymko,² David B. Williams-Young,¹ Norm M. Tubman,³ and Roel Van Beeumen¹

¹*Applied Mathematics and Computational Research Division,
Lawrence Berkeley National Laboratory, Berkeley, CA 94720, USA*

²*National Energy Research Scientific Computing Center,
Lawrence Berkeley National Laboratory, Berkeley, CA 94720, USA*

³*NASA Ames Research Center, Moffett Field, CA 94035, USA*

(Dated: June 19, 2023)

Ground state energy estimation in physics and chemistry is one of the most promising applications of quantum computing. In this paper, we introduce a novel measurement-driven approach that finds eigenenergies by collecting real-time measurements and post-processing them using the machinery of dynamic mode decomposition (DMD). We provide strong theoretical and numerical evidence that our method converges rapidly even in the presence of noise and show that our method is isomorphic to matrix pencil methods developed independently across various scientific communities. Our DMD-based strategy can systematically mitigate perturbative noise and stands out as a promising hybrid quantum-classical eigensolver.

Introduction.—A common goal in chemistry and materials physics is to understand low-energy states, especially the ground state. Strong many-body interactions and an exponential Hilbert space make this problem extremely challenging on classical computers, leading to growing interest in quantum approaches [1, 2]. However, fully quantum algorithms for eigenvalue estimation [3] require fault-tolerant resources beyond near-term capabilities, and existing hybrid quantum-classical algorithms are susceptible to noise or require demanding classical processing [4, 5].

Recently, several quantum algorithms for Hamiltonian spectral estimation have been proposed, which involve the quantum measurement of appropriate Hamiltonian and overlap matrix elements followed by the classical solution of a generalized eigenvalue problem [6]. Many of these methods generate non-orthogonal expansion states using real [7–12] or imaginary [13] time evolution and diagonalize the Hamiltonian within the Krylov subspace [14, 15] spanned by these states. Real-time methods are particularly promising in the near term because unitary evolution is native on a quantum computer. However, the non-orthogonality of the expansion states typically leads to an ill-conditioned generalized eigenvalue problem [9, 10], a difficulty exacerbated by the presence of noise on quantum hardware.

One can address the classical ill-conditioning in these hybrid algorithms by examining the long history in numerical linear algebra dedicated to solving such near-singular problems [16]. Starting from the seminal efforts of Prony in 1795 [17], there has been extensive work on matrix pencil methods [18–30] that exploit various rank factorization and signal subspace properties, aiming to ensure the robustness of the solution. For example, the celebrated Prony’s method decomposes a sparse signal into oscillatory modes by resolving the principal frequen-

cies of a linear time-invariant system [31]. The method was recently revisited in the context of quantum signal processing for phase factorization [32].

Here we extend these methods by showing that the more recent dynamic mode decomposition (DMD) technique [33–37] can be used to effectively tackle the ill-conditioning in a noise-resilient way. We provide a unified framework built on Takens’ embedding technique [38–40] and the DMD formalism. Standard DMD characterizes the state of a dynamical system based on observation at a single previous timestep; a variant, higher-order dynamic mode decomposition (HODMD) [41], utilizes several past timesteps instead. In our approach, we use a number of timesteps for each characterization as in HODMD, but we monitor a single observable rather than the full system state; we hence refer to our method as observable-DMD (ODMD), and demonstrate its efficacy numerically on a range of chemically relevant Hamiltonians.

We make several key contributions: (1) we show how to extend the DMD formalism to the quantum realm, where we have access only to the observables and not to the full states; (2) we demonstrate that this approach can be employed in a quantum hardware-efficient manner to estimate eigenenergies, and we provide strong theoretical and numerical evidence that our estimator converges rapidly even in the presence of noise; and (3) we show that our method maps isomorphically to modern matrix pencil methods developed independently across a variety of scientific communities, generalizing the sparse reconstruction idea pioneered by Prony centuries ago.

Observable-DMD.—Standard DMD is a measurement-driven approximation that samples snapshots of the system at regular time intervals Δt and uses them to construct an efficient linear representation of the dynamical trajectory. The optimal linear approximation for the step

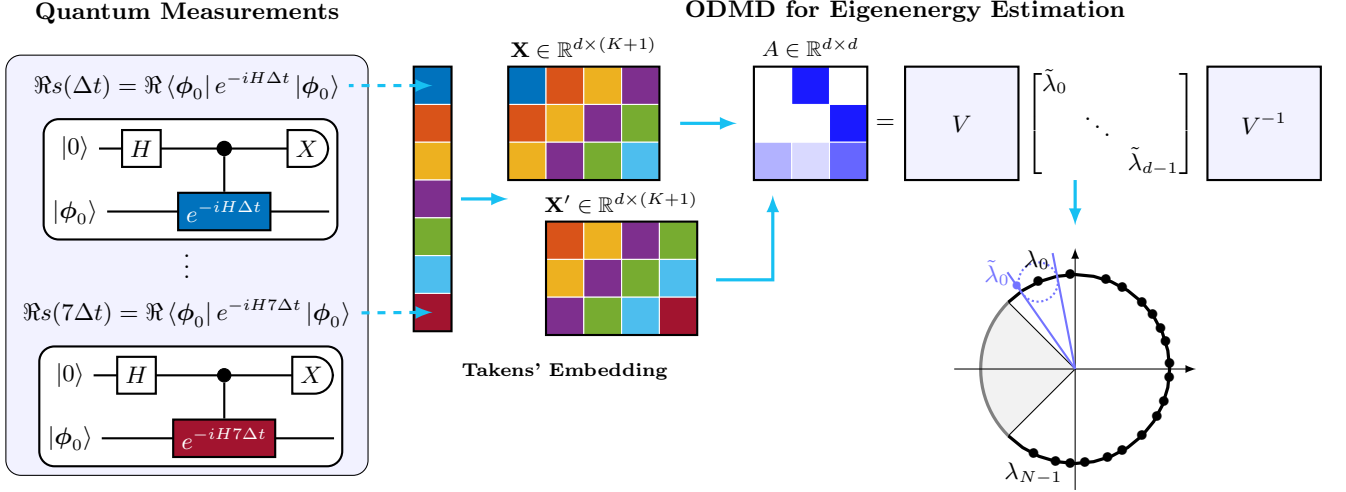


FIG. 1. ODMD applied to eigenenergy estimation. ODMD uses the real (or imaginary) part of the expectation of the time evolution operator, $s(k\Delta t) = \langle \phi_0 | e^{-iHk\Delta t} | \phi_0 \rangle$, with respect to some reference state $|\phi_0\rangle$. This data can be measured efficiently on a quantum processor, for example by means of the Hadamard test. ODMD constructs a pair of Hankel matrices \mathbf{X}, \mathbf{X}' using Takens' embedding and generates the DMD system matrix A of companion structure (matrix elements of the same color are equal). Under mild assumptions on Δt , the eigenvalue $\tilde{\lambda}_0$ of A with $\arg(\tilde{\lambda}_0) = \max_\ell \arg(\tilde{\lambda}_\ell)$ converges to the true ground state phase λ_0 as the size of \mathbf{X}, \mathbf{X}' increases. The ground state energy is then estimated as $\tilde{E}_0 = -\arg(\tilde{\lambda}_0)/\Delta t$.

$k \mapsto k+1$ is expressed as $\phi_{k+1} \stackrel{\text{LS}}{=} A_k \phi_k$, where $\phi_k \in \mathbb{C}^{d_s}$ is the state of a system and $A_k \in \mathbb{C}^{d_s \times d_s}$ is the k th-step system matrix, *i.e.*, the linear operator that minimizes the residual $\|\phi_{k+1} - A_k \phi_k\|_2$, yielding the least-squares (LS) equality. Similarly, an optimal linear approximation for a sequence of successive snapshots $k = 0, 1, \dots, K+1$ can be determined from the solution,

$$\begin{bmatrix} | & | & & | \\ \phi_1 & \phi_2 & \cdots & \phi_{K+1} \\ | & | & & | \end{bmatrix} \stackrel{\text{LS}}{=} A \begin{bmatrix} | & | & & | \\ \phi_0 & \phi_1 & \cdots & \phi_K \\ | & | & & | \end{bmatrix}, \quad (1)$$

where the system matrix A minimizes the sum of squared residuals over the sequence. The matrix A naturally generates an approximate linear flow governed by its eigenmodes. DMD-based approaches can be remarkably effective despite their simplicity, since they are deeply rooted in the Koopman operator theory describing the general (non)linear dynamics of operators [42–46].

The DMD characterization of the system evolution described above requires complete knowledge of the state. However, a quantum computer can only provide access to the state via measurement sampling of observables [47]. Moreover, the state at each timestep in Eq. (1) consists of d_s complex numbers, while each quantum measurement yields only a single real number; we thus need to suitably augment our measurements to retrieve a sufficiently descriptive system matrix.

We address these challenges by employing Takens' embedding (TE) technique [38–40] in tandem with the linear model underpinning DMD. The TE theorem [38, 39] relates an m -dimensional (sub)manifold of states, which observers cannot directly access, to a sequence of at most

$d = 2m + 1$ time-delayed measurements of an observable, which identifies the system dynamics. This correspondence reads $\phi(t) \leftrightarrow o_t$, where $\phi(t)$ is the system state and $o_t = [o(t), o(t + \Delta\tau), \dots, o(t + (d-1)\Delta\tau)]^\top$ is a d -dimensional “observable history” vector of measured observables $o(t) = o[\phi(t)]$ separated by time delay $\Delta\tau$.

Suppose that at time-steps $\{t_k = k\Delta t\}_{k=0}^{K+1}$ we acquire a sequence of observable histories $\{o_{t_k}\}_{k=0}^{K+1}$. For efficient usage of near-term resources, we pick $\Delta\tau = \Delta t$ such that $K + d + 1$ observables measured at times $\{k\Delta t\}_{k=0}^{K+d}$ simultaneously give all $K + 2$ observable-histories,

$$o_k := o_{t_k} = \begin{bmatrix} o(t_k) \\ o(t_{k+1}) \\ \vdots \\ o(t_{k+d-1}) \end{bmatrix}, \quad 0 \leq k \leq K+1. \quad (2)$$

By construction, the first $(d-1)$ entries of o_k are identical to the last $(d-1)$ entries of o_{k-1} . As a consequence, the matrix $\mathbf{O}_{1:k} = [o_{k_1} \ o_{k_1+1} \ \cdots \ o_{k_d}]$ formed by taking successive o_k as columns has a Hankel structure, *i.e.*, the matrix elements on each anti-diagonal are equal. In the embedding space, we can identify the closest linear flow,

$$\mathbf{O}_{1:K+1} \stackrel{\text{LS}}{=} A \mathbf{O}_{0:K} \implies A = \mathbf{O}_{1:K+1} (\mathbf{O}_{0:K})^+, \quad (3)$$

where $+$ denotes the Moore–Penrose pseudo-inverse. For the case $\Delta\tau = \Delta t$, the system matrix A assumes a companion structure with just d free parameters (see Fig. 1 and Eq. (24) in the Appendix). The ODMD approximation to the system dynamics is then stored in these d parameters, which are optimally inferred from the $K + d + 1$ measured observables.

Algorithm 1: ODMD ground state energy estim.

Input: Timestep Δt , embedding dimensions $\{d_k\}_{k \geq 0}$.
Output: Estimated ground state energy \tilde{E}_0 .

```

1   $k = 0$ .
2  while not converged do
3     $\Re s_k = \Re(s(k\Delta t))$ ; /* quantum measurement */
4     $\mathbf{X}, \mathbf{X}' \leftarrow TE(\Re s_0, \dots, \Re s_k; d_k)$ 
5     $A \leftarrow \mathbf{X}' \mathbf{X}^+$ ; /* update system matrix */
6     $\tilde{E}_0 \Delta t \leftarrow -\max_{1 \leq \ell \leq d_k} \Im \log(\tilde{\lambda}_\ell)$ ; /* update energy */
7     $k \leftarrow k + 1$ 
end

```

ODMD for Eigenenergy Estimation.—We now specialize the ODMD method in pursuit of a compact and robust eigenenergy estimator for quantum systems. With Hamiltonian H , the dynamics are given by the time evolution operator e^{-iHt} (with the convention of $\hbar = 1$). We consider as our observable the complex-valued overlap,

$$s(t) = \langle \phi_0 | e^{-iHt} | \phi_0 \rangle, \quad (4)$$

whose real and imaginary parts can be separately measured, *e.g.*, using the Hadamard test [48]. Upon arranging the time-delayed overlaps into a pair of shifted Hankel matrices $\mathbf{X}, \mathbf{X}' \in \mathbb{C}^{d \times (K+1)}$,

$$\mathbf{X} = \mathbf{S}_{0:K}, \quad \mathbf{X}' = \mathbf{S}_{1:K+1}, \quad (5)$$

the eigenenergies of the Hamiltonian can then be simply estimated by solving the eigenvalue problem,

$$A\psi_\ell = \tilde{\lambda}_\ell \psi_\ell, \quad (6)$$

where $\tilde{\lambda}_0 \approx e^{-iE_0\Delta t}$ with $\arg(\tilde{\lambda}_0) = \max_\ell \arg(\tilde{\lambda}_\ell)$ encodes the DMD approximation to the true ground state phase and hence energy. Our measurement-driven estimation is outlined in Algorithm 1, which takes as input the timestep Δt and a sequence of delay embedding dimensions $1 = d_0 \leq d_1 \leq \dots \leq d_{K+d-1} \leq K+d$. We consider $d_k = \max(d_{k-1}, \lfloor \alpha k \rfloor)$ for $\alpha = \frac{1}{2}$ throughout the text.

The eigenvalue problem in Eq. (6) above is isomorphic to the following matrix pencil problem,

$$\mathbf{X}' \psi'_\ell = \tilde{\lambda}_\ell \mathbf{X} \psi'_\ell, \quad (7)$$

which allows us to recast DMD methods as factorization-based matrix pencil methods, including the Eigensystem Realization Algorithm (ERA) [23, 24] and Estimation of Signal Parameters via Rotational Invariance Techniques (ESPRIT) [20–22]. This equivalence offers a unified approach towards extracting eigenenergies as signals driven by the hidden quantum dynamics; a full derivation of this equivalence can be found in the Appendix.

Eigenenergy Convergence.—Alongside its algorithmic simplicity, we provide compelling theoretical and numerical evidence of the rapid convergence of the ODMD estimator. Here we present our main convergence analysis that demonstrates efficient estimation of the ground state energy.

We first note that the overlap can always be expressed as a sum of complex exponentials,

$$s_k = s(k\Delta t) = \sum_{n=0}^{N-1} p_n \lambda_n^k, \quad (8)$$

where N is the size of Hilbert space, $\lambda_n = e^{-iE_n\Delta t}$ represent the eigenphases accumulated from a single timestep, and $p_n = |\langle n | \phi_0 \rangle|^2$ specify the eigenstate probabilities in the reference state $|\phi_0\rangle$. For the extreme case of sufficient sample data with $d = K+1 = N$,

$$A = V \begin{bmatrix} \lambda_0 & & & \\ & \lambda_1 & & \\ & & \ddots & \\ & & & \lambda_{N-1} \end{bmatrix} V^{-1}, \quad (9)$$

where $(V_{ij})_{i,j=1}^N = \lambda_{i-1}^{j-1}$ is the Vandermonde matrix containing the eigenphases. In this case, the eigenvalue problem of Eq. (6) resolves the entire Hamiltonian spectrum, echoing classic techniques of Prony [17] and Padé [49, 50]. Here we highlight the utility of our estimator as a powerful extension when working with limited data samples $d, K \ll N$. Under the mild assumption that we regulate our timestep Δt to keep the eigenphases in a 2π -window such that

$$(E_{N-1} + E_1 - 2E_0)\Delta t \leq 2\pi, \quad (10)$$

we can show a near-exponential convergence of the energy estimation,

$$|\tilde{E}_0 - E_0| \leq \mathcal{O}(K e^{-\beta d}), \quad (11)$$

where

$$\beta > -\ln \frac{\sin((E_{N-1} - E_1)\Delta t/2)}{\sin((E_{N-1} - E_0)\Delta t/2)}, \quad (12)$$

denotes the leading-order exponent that depends on the normalized spectral gap $(E_1 - E_0)/(E_{N-1} - E_0)$. A proof of the error analysis exploits the minimal residual property of DMD solvers and is elaborated in the Appendix. Finally, we remark that the same convergence analysis holds for the real parts of the overlap due to Euler's identity $\cos(E_n \Delta t) = \frac{1}{2}(\lambda_n + \lambda_n^*)$, implying a 50% reduction in the measurement cost.

Comparison with Other Methods.—When combined with regularizing strategies such as singular value thresholding, the ODMD approach can systematically filter out

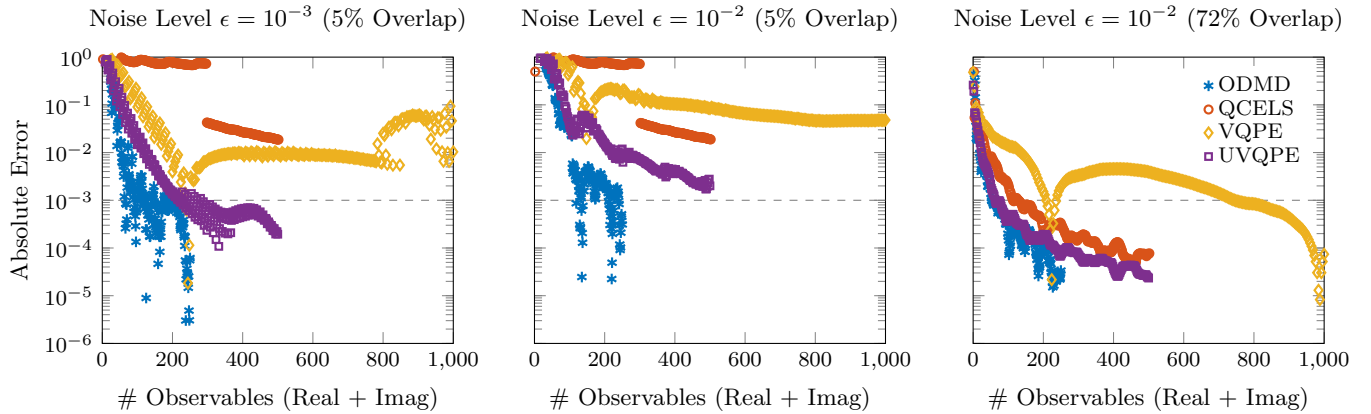


FIG. 2. Absolute error in the Cr_2 ground state energy computed from four state-of-the-art hybrid algorithms based on real-time evolution (ODMD, QCELS, VQPE, UVQPE) as a function of the number of observables, $\langle \phi_0 | e^{-iHk\Delta t} O | \phi_0 \rangle$ with $O = I$ or H , measured. The maximum number of timesteps shown is the same for each algorithm; the maximum number of observables can differ, for example because we count real and imaginary parts separately and ODMD uses only the real part. The three panels exhibit convergence for different values (ϵ , δ , p_0 , Δt) of the noise level ϵ , singular value threshold δ (for ODMD, VQPE, UVQPE), reference-ground overlap probabilities $p_0 = |\langle 0 | \phi_0 \rangle|^2$, and timestep Δt . **Left:** $(10^{-3}, 10^{-2}, 5\%, 1)$; **Center:** $(10^{-2}, 10^{-1}, 5\%, 1)$; and **Right:** $(10^{-2}, 10^{-1}, 72\%, 3)$ (for a Hartree-Fock reference state). The horizontal dashed line indicates chemical accuracy.

noise in the data, thereby making it suitable for extracting spectral and dynamical information from noisy measurements obtained on quantum hardware.

We demonstrate the efficiency of the measurement-driven approach, as inspired by Eqs. (6) and (7), for estimating the ground state energies of strongly-correlated molecular Hamiltonians, a task that holds substantial pragmatic interest in chemical and materials physics. For numerical efficiency, we scale our target Hamiltonian H such that $\|H\|_2 = \pi/4$. Moreover, we introduce Gaussian errors $\mathcal{N}(0, \epsilon^2)$ on the overlap measurements to account for the effect of noise on quantum hardware. Accordingly, we perform singular value thresholding on our data with a set relative threshold $\tilde{\delta} > 0$ to filter out noise, *i.e.*, we truncate singular values smaller than $\tilde{\delta}\sigma_{\max}(\mathbf{X})$ where σ_{\max} defines the largest singular value. Our investigation encompasses molecules of increasing complexity, ranging from the relatively simple LiH to the more challenging Cr_2 (shown in Appendix).

We focus on the ground state energy calculation of Cr_2 , a transition metal dimer known for exhibiting among the strongest electronic correlations. Here we work with a truncated sector of the molecular Hilbert space by employing the adaptive sampling configuration interaction algorithm (ASCI) [51, 52] (see Appendix for further details and examples). Fig. 2 shows the convergence properties of several hybrid quantum-classical real-time algorithms and illuminates the efficacy and noise-resilience of the ODMD approach. We examine recently-developed methods that use similar types of measurements and resources, including subspace expansion techniques exemplified by the Variational Quantum Phase Estimation (VQPE) and its unitary modification (UVQPE) [9],

as well as optimization-based techniques represented by the Quantum Complex Exponential Least Squares (QCELS) [53, 54]. We consider this a crucial initial step in quantifying the performance of different real-time algorithm classes, each developed for unique purposes and aimed at different strategies to leverage the capabilities of current quantum hardware. The three panels display the convergence of estimated energy converted to the original scale, where we examine both small- and large-timestep regimes favoring lower circuit depth and richer dynamical information respectively. The left panel shows a lower noise level and a reference state with small ground state probability $p_0 = |\langle 0 | \phi_0 \rangle|^2 = 0.05 = \max_n p_n$. The blue stars marking the ODMD estimation exhibit satisfying performance compared to the purple squares marking the UVQPE estimation that converges variationally to the true ground state energy in the noiseless limit. The deviation of QCELS estimation, fitted to a uniform-timestep model, results from frustrated optimization as the reference $|\phi_0\rangle$ is almost orthogonal to the target state $|0\rangle$. On the other hand, the right panel shows a higher noise level and a Hartree-Fock reference state with large ground state probability $p_0 > 0.7$. While the ODMD estimation remains noise-resilient, the VQPE estimation displays susceptibility to noise, even when using thresholding strategies, since it tackles the challenge of solving an ill-conditioned generalized eigenvalue problem. The center panel shows an intermediate case with higher noise and small ground state probability. The ODMD estimation is the only one converging past chemical accuracy. Due to a relatively low measurement cost and robust continuous convergence, the ODMD approach emerges as a promising hybrid eigensolver on near-term platforms.

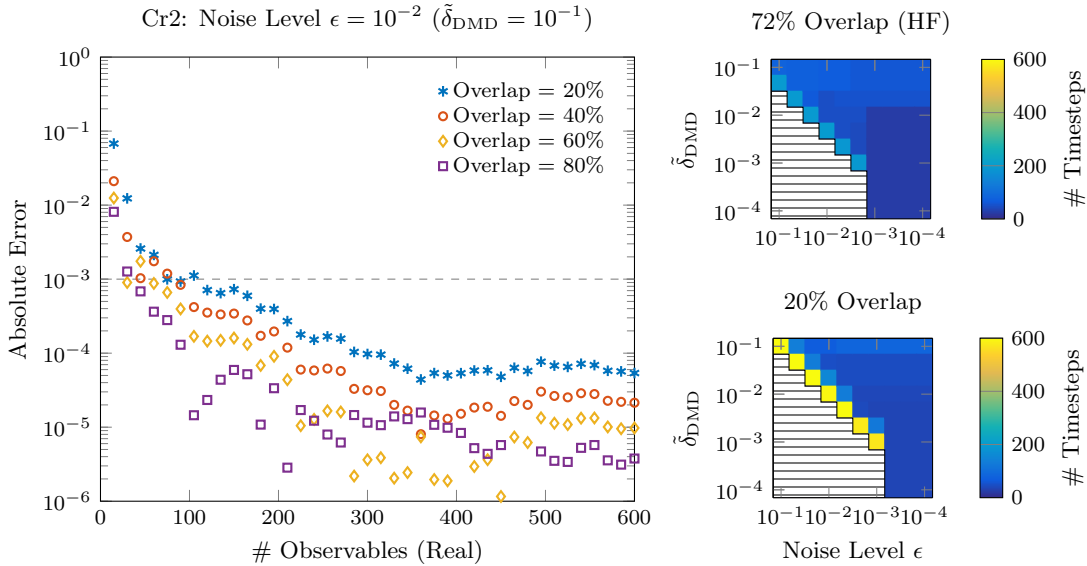


FIG. 3. **Left:** Convergence of the ODMD estimate of the ground state energy for Cr_2 , with overlap measurements given by the exact result $s(t)$ plus Gaussian noise $\mathcal{N}(0, \epsilon^2)$ with standard deviation $\epsilon = 10^{-2}$. A timestep of $\Delta t = 3$ is used for generating the results. The energy converges rapidly even when the reference state $|\phi_0\rangle$ has only 20% overlap probability with the true ground state. In solving the least-squares problem, we filter singular values below the threshold $\tilde{\delta}_{\text{DMD}} = 10^{-1}$. **Right:** The number of DMD timesteps needed to reach chemical accuracy (horizontal dashed line) as a function of the noise level (horizontal axis) and DMD truncation (vertical axis). We consider ground state probabilities of 72% (Hartree-Fock reference state) and 20%. In the black-dotted regions, absolute error remains above chemical accuracy after 750 timesteps.

Fig. 3 further shows the energy convergence of ODMD for varying noise levels, singular value truncation thresholds, and ground state probabilities. The left panel plots the estimation for different reference states with increasing ground state probability. We observe that the ODMD result improves continuously and uniformly for all cases. The right panels show the noise-resistivity of ODMD for specific ground state probabilities $p_0 = 0.2$ and $p_0 > 0.7$. The two panels present the number of timesteps needed to achieve chemical accuracy, highlighting the compactness of our measurement-driven approach.

We note the unified nature of the measurement-driven and matrix pencil method, which exhibit similar convergence as shown in Fig. 6 in the Appendix.

Discussion and Conclusions.—We developed a noise-resilient hybrid quantum-classical algorithm, ODMD, based on real-time evolution for finding eigenenergies of quantum systems. We demonstrated both theoretically and numerically that ODMD converges rapidly with the number of timesteps at which measurements are performed. In particular, the algorithm achieves faster convergence for ground state energy estimation than other related algorithms, including VQPE and QCELS, for the chemical Hamiltonians and initial conditions that we analyzed numerically. The algorithm only requires measurements of the real or imaginary part of the overlap matrix, making it measurement-efficient for near-term quantum hardware. Finally, we have shown that our method is closely related to prominent matrix-factorization meth-

ods developed for applications in signal processing, control theory, and dynamical systems.

This work was funded by the U.S. Department of Energy (DOE) under Contract No. DE-AC0205CH11231, through the Office of Advanced Scientific Computing Research (ASCR) Exploratory Research for Extreme-Scale Science (YS, DC, SD, KK, RVB) and Accelerated Research for Quantum Computing Programs (AS, DBWY). This research used resources of the National Energy Research Scientific Computing Center (NERSC), a U.S. Department of Energy Office of Science User Facility located at Lawrence Berkeley National Laboratory, operated under Contract No. DE-AC02-05CH11231. NMT is grateful for support from NASA Ames Research Center. NMT acknowledge funding from the NASA ARMD Transformational Tools and Technology (TTT) Project.

* yizhis@lbl.gov

[1] S. McArdle, S. Endo, A. Aspuru-Guzik, S. C. Benjamin, and X. Yuan, *Rev. Modern Phys.* **92**, 015003 (2020).
[2] B. Bauer, S. Bravyi, M. Motta, and G. K.-L. Chan, *Chemical Reviews* **120**, 12685 (2020).
[3] A. Y. Kitaev, *Quantum measurements and the Abelian stabilizer problem* (1995).
[4] J. R. McClean, S. Boixo, V. N. Smelyanskiy, R. Babbush, and H. Neven, *Nat. Commun.* **9**, 4812 (2018).

[5] M. Cerezo, A. Arrasmith, R. Babbush, S. C. Benjamin, S. Endo, K. Fujii, J. R. McClean, K. Mitarai, X. Yuan, L. Cincio, *et al.*, *Nat. Rev. Phys.* **3**, 625 (2021).

[6] W. J. Huggins, J. Lee, U. Baek, B. O’Gorman, and K. B. Whaley, *New J. Phys.* **22**, 073009 (2020).

[7] R. M. Parrish and P. L. McMahon, arXiv preprint arXiv:1909.08925 [10.48550/arXiv.1909.08925](https://arxiv.org/abs/1909.08925) (2019).

[8] N. H. Stair, R. Huang, and F. A. Evangelista, *J. Chem. Theory Comput.* **16**, 2236 (2020).

[9] K. Klymko, C. Mejuto-Zaera, S. J. Cotton, F. Wudarski, M. Urbanek, D. Hait, M. Head-Gordon, K. B. Whaley, J. Moussa, N. Wiebe, *et al.*, *PRX Quantum* **3**, 020323 (2022).

[10] E. N. Epperly, L. Lin, and Y. Nakatsukasa, *SIAM J. Matrix Anal. Appl.* **43**, 1263 (2022).

[11] C. L. Cortes and S. K. Gray, *Phys. Rev. A* **105**, 022417 (2022).

[12] Y. Shen, K. Klymko, J. Sud, D. B. Williams-Young, W. A. de Jong, and N. M. Tubman, arXiv preprint arXiv:2208.01063 (2022), <https://arxiv.org/abs/2208.01063>.

[13] M. Motta, C. Sun, A. T. Tan, M. J. O’Rourke, E. Ye, A. J. Minnich, F. G. Brandão, and G. K.-L. Chan, *Nat. Phys.* **16**, 205 (2020).

[14] W. Kirby, M. Motta, and A. Mezzacapo, *Quantum* **7**, 1018 (2023).

[15] N. H. Stair, C. L. Cortes, R. M. Parrish, J. Cohn, and M. Motta, *Phys. Rev. A* **107**, 032414 (2023).

[16] G. H. Golub and C. F. van Loan, *Matrix Computations*, 4th ed. (JHU Press, 2013).

[17] G. Prony, *Journal de l’Ecole Polytechnique* (París) **1**, 24 (1795).

[18] Y. Hua and T. Sarkar, *IEEE Transactions on Acoustics, Speech, and Signal Processing* **38**, 814 (1990).

[19] G. H. Golub, P. Milanfar, and J. Varah, *SIAM J. Sci. Comput.* **21**, 1222 (1999).

[20] R. H. Roy and T. Kailath, *IEEE Trans. Acoust. Speech Signal Process.* **37**, 984 (1989).

[21] L. Auslander, F. Grünbaum, T. Kailath, J. Helton, S. Mitter, U. of Minnesota. Institute for Mathematics, and I. Applications, *Signal Processing: Part II: Control Theory and Applications*, Institute for Mathematics and its Applications Minneapolis, Minn.: +The IMA volumes in mathematics and its applications (Springer New York, 1990).

[22] T. Sarkar and O. Pereira, *IEEE Antennas and Propagation Magazine* **37**, 48 (1995).

[23] R. Pappa and J.-N. Juang, in *25th Structures, Structural Dynamics and Materials Conference* (American Institute of Aeronautics and Astronautics, 1984).

[24] J.-N. Juang and R. S. Pappa, *Journal of Guidance, Control, and Dynamics* **8**, 620 (1985).

[25] E. G. Gilbert, *Journal of The Society for Industrial and Applied Mathematics, Series A: Control* **1**, 128 (1963).

[26] V. Pereyra and G. Scherer, *Exponential Data Fitting and Its Applications* (Bentham eBooks, 2010).

[27] A. Almunif, L. Fan, and Z. Miao, *International Transactions on Electrical Energy Systems* **30**, e12283 (2020).

[28] D. Potts and M. Tasche, *Linear Algebra Appl.* **439**, 1024 (2013).

[29] A. Steffens, P. Rebentrost, I. Marvian, J. Eisert, and S. Lloyd, *New Journal of Physics* **19**, 033005 (2017).

[30] H. Li, H. Ni, and L. Ying, *On low-depth quantum algorithms for robust multiple-phase estimation* (2023).

[31] J. Hauer, C. Demeure, and L. L. Scharf, *IEEE Trans. Power Syst.* **5**, 80 (1990).

[32] L. Ying, *Quantum* **6**, 842 (2022).

[33] I. Mezić and A. Banaszuk, *Physica D: Nonlinear Phenomena* **197**, 101 (2004).

[34] I. Mezić, *Nonlinear Dynamics* **41**, 309 (2005).

[35] C. W. Rowley, I. Mezić, S. Bagheri, P. Schlatter, and D. S. Henningson, *J. Fluid Mech.* **641**, 115 (2009).

[36] P. J. Schmid, *J. Fluid Mech.* **656**, 5–28 (2010).

[37] I. Mezić, *Annu. Rev. Fluid Mech.* **45**, 357 (2013).

[38] D. Ruelle and F. Takens, *Comm. Math. Phys.* **20**, 167 (1971).

[39] F. Takens, in *Lecture Notes in Mathematics* (Springer Berlin Heidelberg, 1981) pp. 366–381.

[40] I. L. Gutiérrez, F. Dietrich, and C. B. Mendl, *Quantum Process Tomography of Unitary Maps from Time-Delayed Measurements* (2021), arXiv:2112.09021 [quant-ph].

[41] S. Le Clainche and J. M. Vega, *SIAM J. Appl. Dyn. Syst.* **16**, 882 (2017).

[42] B. O. Koopman, *Proc. Natl. Acad. Sci. USA* **17** 5, 315 (1931).

[43] G. D. Birkhoff and B. O. Koopman, *Proceedings of the National Academy of Sciences* **18**, 279 (1932).

[44] S. Brunton, B. Brunton, J. Proctor, and J. Kutz, *PLoS one* **11** (2015).

[45] S. L. Brunton, J. L. Proctor, and J. N. Kutz, *Proceedings of the National Academy of Sciences* **113**, 3932 (2016).

[46] H. Arbabi and I. Mezić, *SIAM J. Appl. Dyn. Syst.* **16**, 2096 (2017).

[47] While “observable” is typically used in quantum mechanics to refer specifically to Hermitian operators (with real expectation value), here we use a broader definition, encompassing also complex scalar quantities that can be computed from measurements on a quantum computer.

[48] R. Cleve, A. Ekert, C. Macchiavello, and M. Mosca, *Proc. Roy. Soc. Lond. A* **454**, 339 (1998), arXiv:quant-ph/9708016.

[49] H. Padé, *Annales scientifiques de l’École Normale Supérieure* **9**, 3 (1892).

[50] G. Plonka and M. Tasche, *GAMM-Mitteilungen* **37**, 239.

[51] N. M. Tubman, J. Lee, T. Y. Takeshita, M. Head-Gordon, and K. B. Whaley, *J. Chem. Phys.* **145**, 044112 (2016).

[52] N. M. Tubman, C. D. Freeman, D. S. Levine, D. Hait, M. Head-Gordon, and K. B. Whaley, *J. Chem. Theory Comput.* **16**, 2139 (2020).

[53] Z. Ding and L. Lin, *PRX Quantum* **4**, 020331 (2023).

[54] Z. Ding and L. Lin, *Simultaneous estimation of multiple eigenvalues with short-depth quantum circuit on early fault-tolerant quantum computers* (2023), arXiv:2303.05714 [quant-ph].

[55] N. Akhiezer, *Izv. Kaz. fiz. mat. ob-va* **3** (1928).

[56] K. Schiefermayr, *Acta Scientiarum Mathematicarum* **85**, 629 (2019).

[57] Y. Hua and T. Sarkar, *IEEE Trans. Antennas and Propagation* **37**, 229 (1989).

[58] R. E. Kálmán, *Journal of The Society for Industrial and Applied Mathematics, Series A: Control* **1**, 152 (1963).

[59] J. J. Sanchez-Gasca and J. H. Chow, *IEEE Trans. Power Syst.* **12**, 1461 (1997).

[60] F. Weigend and R. Ahlrichs, *Physical Chemistry Chemical Physics* **7**, 3297 (2005).

- [61] J. S. Binkley, J. A. Pople, and W. J. Hehre, *Journal of the American Chemical Society* **102**, 939 (1980).
- [62] W. J. Hehre, R. F. Stewart, and J. A. Pople, *The Journal of Chemical Physics* **51**, 2657 (1969).

Appendix

We first include brief outlines of standard dynamic mode decomposition and Takens' embedding technique.

Standard Dynamic Mode Decomposition

The standard DMD approach at its core constitutes a data-driven approximation to the time evolution of a dynamical system. Specifically, DMD samples snapshots of the system at regular intervals given by timestep Δt and utilizes them to construct efficient linear representation of the dynamical trajectory. The optimal linear approximation for the step $k \mapsto k + 1$ is expressed as a least-squares (LS) relation,

$$\phi_{k+1} \stackrel{\text{LS}}{=} A_k \phi_k, \quad (13)$$

where $\phi_k \in \mathbb{C}^{d_s}$ is the state of a system and $A_k \in \mathbb{C}^{d_s \times d_s}$ gives the linear operator, also called the k th-step system matrix, that minimizes the residual $\|\phi_{k+1} - A_k \phi_k\|_2$. The optimal linear approximation for a sequence of successive snapshots $k = 0, 1, \dots, K + 1$ can be determined from the solution

$$\begin{bmatrix} | & | & & | \\ \phi_1 & \phi_2 & \cdots & \phi_{K+1} \\ | & | & & | \end{bmatrix} \stackrel{\text{LS}}{=} A \begin{bmatrix} | & | & & | \\ \phi_0 & \phi_1 & \cdots & \phi_K \\ | & | & & | \end{bmatrix}, \quad (14)$$

where the system matrix A here minimizes the sum of squared residuals over the sequence. The optimal linear flow constructed in this way naturally generates an approximate dynamics $\phi_{\text{DMD}}(t) = A^{\frac{t}{\Delta t}} \phi_0$ governed by eigenmodes of the system matrix A . DMD-based approaches can be remarkably effective despite their formal simplicity, as they are rooted in the general Koopman operator theory that characterizes the time evolution of observables under general (non)linear dynamics [42–46].

Takens' Embedding Technique

Takens' embedding theorem [38, 39] establishes a connection between the manifold of states, which observers cannot fully access, and time-delayed measurements of an observable. It states, under generous conditions, that a sequence of at most $d = 2m + 1$ time-delayed measurements identifies the system dynamics on a m -dimensional (sub)manifold of states. This correspondence reads,

$$\phi(t) \leftrightarrow o_t = \begin{bmatrix} o(t) \\ o(t + \Delta\tau) \\ \vdots \\ o(t + (d - 1)\Delta\tau) \end{bmatrix}, \quad (15)$$

where $\phi(t)$ is the system state and $o(t) = o[\phi(t)]$ is the measured observable. The RHS of Eq. (15) is known as a d -dimensional delayed embedding of the observable with a time delay $\Delta\tau$. Takens' theorem relates the evolution of microscopic degrees of freedom with the evolution history of macroscopic observables, providing a concrete probe into the dynamical properties without access to the full state. We use the term Takens' embedding technique to refer to the method of applying time delays on the system observables, motivated by the rigorous results of Takens' embedding theorem.

Next we include a comprehensive proof of the convergence bound from the main text and derive the formal reduction of the DMD-based method to prominent matrix pencil methods.

Generalized Extension to Prony's Method

Prony's method [17] is a pioneering classic approach that has laid the foundation for many modern signal processing and recovery techniques. To understand its underlying idea, let us consider the task of extracting principal frequency components from temporally uniform samples,

$$s_k = \sum_{n=0}^{N-1} p_n e^{-i E_n k \Delta \tau} = \sum_{n=0}^{N-1} p_n \lambda_n^k = \left(\sum_{\Omega} + \sum_{\Omega^c} \right) p_n \lambda_n^k, \quad (16)$$

where $p_n = |\langle n | \phi_0 \rangle|^2$ so that $\sum_n p_n = 1$, $\Omega \subseteq [N] = \{0, 1, \dots, N-1\}$ denotes a set of $|\Omega| \ll N$ eigenindices satisfying $\sum_{n \in \Omega} p_n \gg \sum_{n \in \Omega^c} p_n$, and $\Omega^c = [N] \setminus \Omega$ denotes the complement of Ω . For simplicity, let us assume $\Omega = [d]$. Recall that the eigenvalues are the zeros of the characteristic polynomial

$$\mathcal{C}_{\Omega}(z) = \prod_{\ell \in \Omega} (z - \lambda_{\ell}) = \sum_{\ell=0}^d c_{\ell} z^{\ell}, \quad (17)$$

where $\{c_{\ell}\}_{\ell=0}^d$ are a set of monomial coefficients that depend on $\{\lambda_{\ell}\}_{\ell \in \Omega}$ with the convention $c_d \equiv 1$. Next, observe that evaluating Eq. (17) at the samples (16), i.e., $\mathcal{C}_{\Omega}(z = s_k)$ for $k \geq 0$, yields

$$\sum_{\ell=0}^d c_{\ell} s_{\ell+k} = \sum_{\ell=0}^d c_{\ell} \sum_{n=0}^{N-1} p_n \lambda_n^{\ell+k}, \quad (18)$$

$$= \sum_{n=0}^{N-1} p_n \lambda_n^k \sum_{\ell=0}^d c_{\ell} \lambda_n^{\ell} = \sum_{n=0}^{N-1} p_n \lambda_n^k \mathcal{C}_{\Omega}(\lambda_n), \quad (19)$$

$$= \sum_{n=d}^{N-1} p_n \lambda_n^k \mathcal{C}_{\Omega}(\lambda_n) := r_{k,\Omega}, \quad (20)$$

where the sum $\sum_{n < d}$ vanishes since $\mathcal{C}_{\Omega}(\lambda_n) \equiv 0$ for $n < d$. By using the triangle inequality, the residual term $r_{k,\Omega}$ can be bounded uniformly from above

$$|r_{k,\Omega}| \leq \sum_{n \in \Omega^c} p_n |\mathcal{C}_{\Omega}(\lambda_n)| \leq \max_{n \in \Omega^c} |\mathcal{C}_{\Omega}(\lambda_n)| \sum_{n \in \Omega^c} p_n \leq \|\vec{c}\|_1 \sum_{n \in \Omega^c} p_n, \quad (21)$$

so

$$\sum_{\ell=0}^{d-1} c_{\ell} s_{\ell+k} = -s_{d+k} + r_{k,\Omega} \approx -s_{d+k}, \quad (22)$$

when $\|\vec{c}\|_1 \sum_{n \in \Omega^c} p_n \ll 1$. In matrix form, the evolution of $\{s_k\}_{d \leq k \leq K+d}$ for some $K \in \mathbb{N}$ therefore follows

$$\begin{bmatrix} s_0 & s_1 & \cdots & s_{d-1} \\ s_1 & s_2 & \cdots & s_d \\ \vdots & \vdots & \ddots & \vdots \\ s_K & s_{K+1} & \cdots & s_{K+d-1} \end{bmatrix} \begin{bmatrix} c_0 \\ c_1 \\ \vdots \\ c_{d-1} \end{bmatrix} = - \begin{bmatrix} s_d \\ s_{d+1} \\ \vdots \\ s_{K+d} \end{bmatrix} + \begin{bmatrix} r_{0,\Omega} \\ r_{1,\Omega} \\ \vdots \\ r_{K,\Omega} \end{bmatrix}, \quad (23)$$

which describes the linear time-invariant dynamics,

$$\underbrace{\begin{bmatrix} s_1 & s_2 & \cdots & s_{K+1} \\ s_2 & s_3 & \cdots & s_{K+2} \\ \vdots & \vdots & \ddots & \vdots \\ s_d & s_{d+1} & \cdots & s_{K+d} \end{bmatrix}}_{\mathbf{x}'} \approx \underbrace{\begin{bmatrix} 0 & & & \\ \vdots & I_{d-1} & & \\ 0 & & & \\ \hline -c_0 & -c_1 & \cdots & -c_{d-1} \end{bmatrix}}_A \underbrace{\begin{bmatrix} s_0 & s_1 & \cdots & s_K \\ s_1 & s_2 & \cdots & s_{K+1} \\ \vdots & \vdots & \ddots & \vdots \\ s_{d-1} & s_d & \cdots & s_{K+d-1} \end{bmatrix}}_{\mathbf{x}}, \quad (24)$$

where $\mathbf{X}, \mathbf{X}' \in \mathbb{C}^{d \times (K+1)}$ are time-delayed Hankel matrices, $A \in \mathbb{C}^{d \times d}$ is a system matrix of companion structure, and $I_{d-1} \in \mathbb{C}^{(d-1) \times (d-1)}$ denotes the identity matrix. For interested readers, the connection between the characteristic polynomial \mathcal{C}_Ω and the associated linear recurrence relation above are explicitly discussed in Lemma 2.2 from Ref [28]. Prony's method essentially solves for the monomial coefficients \vec{c} and thus the eigenfrequencies $\{\lambda_n\}_{n \in \Omega}$ as the roots of \mathcal{C}_Ω when Eqs. (23) and (24) hold exact for $N = d$ (so that $r_{k,\Omega} \equiv 0$).

Here, we consider the dynamic mode decomposition (DMD) approach formulated in Eq. (14) as a powerful extension of Prony's method when $d \ll N$, which solves the linear least-squares (LLSQ) problems of the same type, *i.e.*, $\mathbf{X}' = A\mathbf{X}$, where $A = \arg \min_{\tilde{A} \in \mathbb{C}^{d \times d}} \|\mathbf{X}' - \tilde{A}\mathbf{X}\|_F^2$. In other words, the DMD post-processing identifies the set of monomial coefficients $\vec{a} \approx \vec{c}$ that minimize the total residual. Let

$$\mathcal{C}_{\text{DMD}}(z) = \prod_{\ell=0}^{d-1} (z - \tilde{\lambda}_\ell) = \sum_{\ell=0}^d a_\ell z^\ell, \quad (25)$$

represent the characteristic polynomial corresponding to the system matrix A , with $a_d \equiv 1$. Then, we define the DMD residual as follows

$$r_{k,\text{DMD}} = \sum_{n=0}^{N-1} p_n \lambda_n^k \mathcal{C}_{\text{DMD}}(\lambda_n), \quad (26)$$

p_n and λ_n are given in Eq. (16). Note that in case $\tilde{\lambda}_n \approx \lambda_n$, for $n = 0, 1, \dots, d-1$, the contribution of the d first terms in Eq. (26) will remain minimal. In fact, we may now show that the eigenvalues $\{\tilde{\lambda}_\ell\}_{\ell=0}^{d-1}$ of the DMD system matrix A well approximate the target eigenvalues $\{\lambda_n\}_{n \in \Omega}$ for some Ω .

Let \mathcal{P}_d be the set of polynomials of at most degree d and $\mathcal{P}'_d \subset \mathcal{P}_d$ the set of monic polynomials, *i.e.*, $\mathcal{P}'_d = \{\mathcal{C} \in \mathcal{P}_d : \mathcal{C} - z^d \in \mathcal{P}_{d-1}\}$. For any polynomial $\mathcal{C} \in \mathcal{P}_d$, the triangle inequality implies

$$\left| \sum_{n=0}^{N-1} p_n \lambda_n^k \mathcal{C}(\lambda_n) \right| \leq \sum_{n=0}^{N-1} p_n |\mathcal{C}(\lambda_n)|, \quad (27)$$

which allows us to establish a uniform upper bound on the DMD residual

$$\sum_{k=0}^K |r_{k,\text{DMD}}|^2 = \min_{\mathcal{C} \in \mathcal{P}'_d} \sum_{k=0}^K \left| \sum_{n=0}^{N-1} p_n \lambda_n^k \mathcal{C}(\lambda_n) \right|^2, \quad (28)$$

$$\leq (K+1) \min_{\mathcal{C} \in \mathcal{P}'_d} \left(\sum_{n=0}^{N-1} p_n |\mathcal{C}(\lambda_n)| \right)^2, \quad (29)$$

$$\leq (K+1) \min_{\mathcal{C} \in \mathcal{P}'_d} \max_{0 \leq n \leq N-1} |\mathcal{C}(\lambda_n)|^2. \quad (30)$$

We now proceed by saturating a tight bound on the DMD residual through the min-max inequality above. Given our freedom to pick the time increment $\Delta\tau$ such that $(E_{N-1} - E_0)\Delta\tau = 2\Theta \leq 2\pi$, we further bound the RHS of Eq. (30) via polynomials over the circular arc $\mathcal{A}_\Theta = \{z \in \mathbb{C} : |z| = 1, -\Theta \leq \arg(z) \leq \Theta\}$. An example of such circular arc with $\Theta = \pi/2$ is sketched in Fig. 4 below.

In particular, let us consider the choice of complex-valued Chebyshev polynomials,

$$\hat{\mathcal{C}}(z) = \arg \min_{\mathcal{C} \in \mathcal{P}'_d} \sup_{z \in \mathcal{A}_\Theta} |\mathcal{C}(z)|, \quad (31)$$

whose parametric representations can be explicitly constructed from tools such as Jacobi's elliptic and theta functions [55]. For notational convenience, we define $\|\mathcal{C}(z)\|_\Theta = \sup_{z \in \mathcal{A}_\Theta} |\mathcal{C}(z)|$. Similar to real-valued Chebyshev polynomials over the unit interval, $\hat{\mathcal{C}}(z)$ retains the minimal norm property on \mathcal{A}_Θ with

$$\|\hat{\mathcal{C}}\|_\Theta \sim 2 \sin^d(\Theta/2) \cos^2(\Theta/4), \quad (32)$$

asymptotically for large d [56]. Consequently, the difference in residuals associated with the Prony-like and DMD

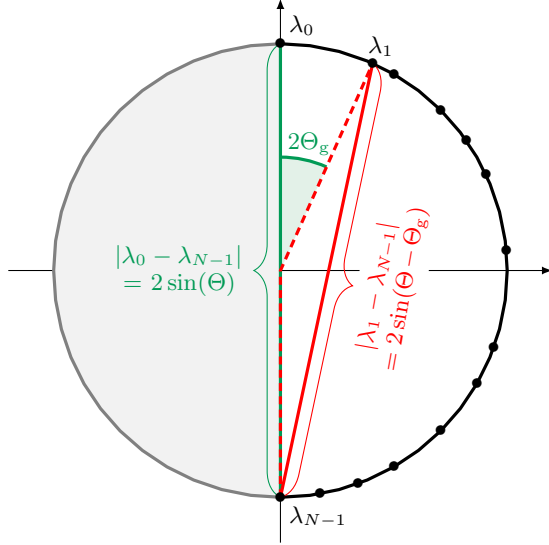


FIG. 4. Characteristic polynomial \mathcal{C}_Ω with roots along the arc $\mathcal{A}_{\Theta=\pi/2}$ and $0 \in \Omega$. The eigenphases $\{\lambda_n\}_{n=0}^{N-1}$ are represented schematically by black dots on the unit circle. Geometrically, $\|\tilde{\mathcal{C}}_{\Omega \setminus \{0\}}\|_{\Theta-\Theta_g}$ is bounded by the solid red chord of length $|\lambda_1 - \lambda_{N-1}| = 2 \sin(\Theta - \Theta_g)$, whereas $\|\mathcal{C}_\Omega\|_\Theta$ is bounded by the green solid chord of length $|\lambda_0 - \lambda_{N-1}| = 2 \sin(\Theta)$. Our strategy for selecting appropriate reference eigenindex set Ω is aimed at minimizing $\|\tilde{\mathcal{C}}_{\Omega \setminus \{0\}}\|_{\Theta-\Theta_g} / |\partial_z \mathcal{C}_\Omega(\lambda_0)|$, where $|\partial_z \mathcal{C}_\Omega(\lambda_0)| \approx \|\mathcal{C}_\Omega\|_\Theta^{d-1}$ for $\{\lambda_{n_\ell}\}_{\ell=1}^{d-1}$ far away from λ_0 . Note that $\tilde{\mathcal{C}}_{\Omega \setminus \{0\}}$ undergoes a global phase shift of $e^{-i\Theta_g}$ relative to $\mathcal{C}_{\Omega \setminus \{0\}}$, which center the arc $\mathcal{A}_{\Theta-\Theta_g}$ around $z=1$.

linear systems of the type Eq. (23) can be bounded as,

$$\|\vec{r}_\Omega - \vec{r}_{\text{DMD}}\|_2^2 = \sum_{k=0}^K |r_{k,\Omega} - r_{k,\text{DMD}}|^2, \quad (33)$$

$$\leq 2 \sum_{k=0}^K |r_{k,\Omega}|^2 + 2 \sum_{k=0}^K |r_{k,\text{DMD}}|^2, \quad (34)$$

$$\leq 2 \sum_{k=0}^K \max_{1 \leq n \leq N-1} |\mathcal{C}_\Omega(\lambda_n)|^2 + 2 \sum_{k=0}^K |r_{k,\text{DMD}}|^2, \quad (35)$$

where we now work with a generic set $\Omega = \{n_0 = 0, n_1, \dots, n_{d-1}\}$ of d eigenindices. Eq. (34) follows from the application of triangle and Cauchy–Schwarz inequalities $|z - z'|^2 \leq |z|^2 + 2|z||z'| + |z'|^2 \leq 2|z|^2 + 2|z'|^2$ while Eq. (35) exploits the upper bound derived in Eq. (21). Using the minimal norm property of the DMD residual, we have

$$\|\vec{r}_\Omega - \vec{r}_{\text{DMD}}\|_2^2 \leq 2(K+1) \max_{1 \leq n \leq N-1} |\mathcal{C}_\Omega(\lambda_n)|^2 + 2(K+1) \min_{\mathcal{C} \in \mathcal{P}'_d} \max_{0 \leq n \leq N-1} |\mathcal{C}(\lambda_n)|^2, \quad (36)$$

$$\leq 2(K+1) \left[\max_{1 \leq n \leq N-1} |\lambda_n - \lambda_0|^2 \max_{1 \leq n \leq N-1} \left| \prod_{\ell=1}^{d-1} (\lambda_n - \lambda_{n_\ell}) \right|^2 + \|\hat{\mathcal{C}}\|_\Theta^2 \right], \quad (37)$$

$$\leq 2(K+1) \left[\left(2 \max_{1 \leq n \leq N-1} \left| \prod_{\ell=1}^{d-1} (\lambda_n - \lambda_{n_\ell}) \right| \right)^2 + \|\hat{\mathcal{C}}\|_\Theta^2 \right], \quad (38)$$

$$\leq 2(K+1) \left[2 \|\tilde{\mathcal{C}}_{\Omega \setminus \{0\}}\|_{\Theta-\Theta_g} + \|\hat{\mathcal{C}}\|_\Theta^2 \right]^2, \quad (39)$$

where $\Theta_g = (E_1 - E_0)\Delta\tau/2$ represents the dimensionless ground state and first excited state angle. It is worth noting that we can always assume $\Theta_g > 0$ since otherwise $p_0\lambda_0^k + p_1\lambda_1^k = (p_0 + p_1)\lambda_0^k \implies N \mapsto N-1$ and $\{E_n\}_{n=1}^{N-1} \mapsto \{E_{n-1}\}_{n=1}^{N-1}$. For notational consistency, we let $\tilde{\mathcal{C}}_{\Omega \setminus \{0\}}(z) = \prod_{\ell=1}^d (e^{-i\Theta_g} z - \lambda_{n_\ell}) \in \mathcal{P}_{d-1}$ denote the polynomial of degree $(d-1)$ with a proper phase shift included. Since $\|\hat{\mathcal{C}}\|_\Theta$ is optimally bounded, next we show that

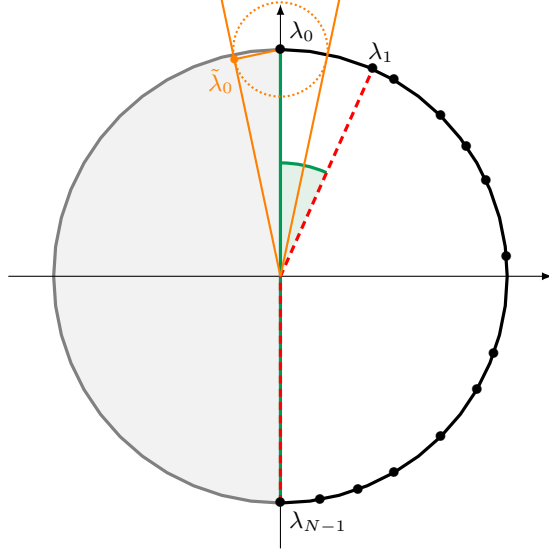


FIG. 5. Error in the ground state energy inferred from error in the ground state eigenphase. The eigenphases $\{\lambda_n\}_{n=0}^{N-1}$ are shown schematically as black dots on the unit circle. The dotted orange circle indicates an upper bound on the eigenphase difference $|\tilde{\lambda}_0 - \lambda_0|$. Deviation in the angles $|\tilde{E}_0 - E_0|\Delta\tau$ can be determined through the construction of tangent lines to the orange circle centered at λ_0 .

$\|\tilde{\mathcal{C}}_{\Omega \setminus \{0\}}\|_{\Theta - \Theta_g}$ can also be bounded in a controlled way. Specifically, we claim that there exists $(\Theta_0, \Theta_1) \subseteq [0, \pi]$ so that $\forall \Theta \in [\Theta_0, \Theta_1]$, $\|\tilde{\mathcal{C}}_{\Omega \setminus \{0\}}\|_{\Theta - \Theta_g} \ll 2^{d-1}$ asymptotically for a collection of index sets: for concreteness, we examine the example $\Theta = \pi/2$ and $\Omega \setminus \{0\} = \{n_\ell\}_{\ell=1}^{d-1}$ which clusters around the antipodal point of λ_0 , *i.e.*, $\lambda_{n_\ell} \approx -\lambda_0, \forall \ell \neq 0$. A direct calculation shows that

$$|z - \lambda_{n_\ell}| = 2 \sin \left| \frac{\arg(z) - \arg(\lambda_{n_\ell})}{2} \right| \implies \|\tilde{\mathcal{C}}_{\Omega \setminus \{0\}}\|_{\pi/2 - \Theta_g} \sim 2^{d-1} \sin^{d-1}(\pi/2 - \Theta_g), \quad (40)$$

Graphically, Fig. 4 helps elucidate the bounded behavior of \mathcal{C}_Ω and thereby $\tilde{\mathcal{C}}_{\Omega \setminus \{0\}}$ in the presence of the spectral gap Θ_g .

Going forward, for the sake of illustration, let us restrict our attention to any index set Ω that admits near maximal product of distances $\prod_{\ell=1}^{d-1} |\lambda_0 - \lambda_{n_\ell}|$. Recall from Eq. (23) that $\vec{a} - \vec{c} = \mathbf{X}^\top (\vec{r}_\Omega - \vec{r}_{\text{DMD}})$. Thus combining our previous results, we see that the DMD coefficients \vec{a} and the target coefficients \vec{c} converge towards each other at an rate,

$$\|\vec{a} - \vec{c}\|_2 \lesssim \|(\mathbf{X}^\top)^+\|_2 \|\vec{r}_\Omega - \vec{r}_{\text{DMD}}\|_2, \quad (41)$$

$$\leq \frac{[2(K+1)]^{1/2} \{ 2\|\tilde{\mathcal{C}}_{\Omega \setminus \{0\}}\|_{\Theta - \Theta_g} + \|\hat{\mathcal{C}}\|_\Theta \}}{\delta}, \quad (42)$$

where recall that $\mathbf{X} \in \mathbb{C}^{d \times (K+1)}$ is the data matrix and $\delta > 0$ denotes a lower bound on its singular values. To monitor the scaling of our DMD approximation, we write $d = \lfloor \alpha(K+1) \rfloor$ for which $0 \leq \alpha \leq 1$ is kept constant throughout (here it suffices to discuss $0 \leq \alpha \leq 1$ due to the Hankel structure of our data matrix). Moreover, previous literature supports the common practice of working with $\alpha \lesssim 1$ as near-optimal choice [18, 57]. The error in the ground state energy can then be estimated and analyzed through first-order perturbation theory,

$$\partial_{c_\ell} \mathcal{C}_\Omega(\lambda_0) = 0, \forall \ell \iff \lambda_0^\ell + \sum_{k=1}^d c_k k (\lambda_0)^{k-1} \partial_{c_\ell} \lambda_0 = 0, \quad (43)$$

$$\iff \partial_{c_\ell} \lambda_0 = -\frac{\lambda_0^\ell}{\partial_z \mathcal{C}_\Omega(\lambda_0)}, \quad (44)$$

so we have $\tilde{\lambda}_0 - \lambda_0 = \sum_{\ell=0}^{d-1} (a_\ell - c_\ell) \partial_{c_\ell} \lambda_0$ up to leading order and,

$$|\tilde{\lambda}_0 - \lambda_0| = \left| \frac{\sum_{\ell=0}^{d-1} (a_\ell - c_\ell) \lambda_0^\ell}{\partial_z \mathcal{C}_\Omega(\lambda_0)} \right| \leq \frac{\|\vec{a} - \vec{c}\|_1}{\prod_{\ell \in \Omega \setminus \{0\}} |\lambda_0 - \lambda_\ell|}, \quad (45)$$

$$\leq \frac{(2\alpha)^{1/2}(K+1) \left\{ 2\|\tilde{\mathcal{C}}_{\Omega \setminus \{0\}}\|_{\Theta - \Theta_g} + \|\hat{\mathcal{C}}\|_\Theta \right\}}{\delta \prod_{\ell \in \Omega \setminus \{0\}} 2|\sin(\theta_{0\ell})|}, \quad (46)$$

where we use the norm inequality $\|\vec{a} - \vec{c}\|_1 \leq d^{1/2} \|\vec{a} - \vec{c}\|_2$ and define the eigenangle variables $\theta_{j\ell} = (E_\ell - E_j) \Delta\tau/2$. Here we order the DMD eigenvalues $\{\tilde{\lambda}_0, \dots, \tilde{\lambda}_{d-1}\}$ based on their arguments in a descending order, *i.e.*, $\arg \tilde{\lambda}_0 \geq \arg \tilde{\lambda}_1 \geq \dots \geq \arg \tilde{\lambda}_{d-1}$, so that $\tilde{\lambda}_0 \approx \lambda_0$ contains the ground state information. For the case $\Theta_0 \leq \Theta \leq \pi/2$, we note that picking $\theta_{0\ell} \sim 2\Theta$ gives $|\sin(\theta_{0\ell})| \sim \sin(\Theta)$. Therefore Eq. (46) can be bounded asymptotically as,

$$|\tilde{\lambda}_0 - \lambda_0| \lesssim \frac{(2\alpha)^{1/2}(K+1)}{\delta 2^{d-1} \sin^{d-1}(\Theta)} \left\{ 2\|\tilde{\mathcal{C}}_{\Omega \setminus \{0\}}\|_{\Theta - \Theta_g} + \|\hat{\mathcal{C}}\|_\Theta \right\}, \quad (47)$$

$$\leq \frac{2^{3/2}\alpha^{1/2}(K+1)}{\delta 2^{d-1} \sin^{d-1}(\Theta)} \left\{ 2^{d-1} \sin^{d-1}(\Theta - \Theta_g) + \sin^d(\Theta/2) \cos^2(\Theta/4) \right\}, \quad (48)$$

$$\approx \frac{2^{3/2}\alpha^{1/2}K}{\delta} \left[\frac{\sin^\alpha(\Theta - \Theta_g)}{\sin^\alpha(\Theta)} \right]^K \quad (49)$$

$$+ \frac{2^{3/2}\alpha^{1/2}K \sin(\Theta_1/2) \cos^2(\Theta_0/4)}{\delta (2^\alpha)^K} \left[\frac{\sin^\alpha(\Theta/2)}{\sin^\alpha(\Theta)} \right]^K, \quad (50)$$

with $K \gg 1$. Since typically $\Theta > 2\Theta_g$ for practical Hamiltonians, it follows that the leading term in Eq. (50) decays proportional to $Ke^{-\beta_1 K}$ where $\beta_1(\Theta, \Theta_g) = -\alpha \ln[\sin(\Theta - \Theta_g)/\sin(\Theta)] > 0$ and the subleading term decays proportional to $Ke^{-\beta_2 K}$ where $\beta_2(\Theta) = -\alpha \ln[\sin(\Theta/2)/2\sin(\Theta)] > \beta_1 > 0$. Finally using a simple tangent line argument as sketched in Fig. 5, we have for sufficiently small $|\tilde{\lambda}_0 - \lambda_0|$,

$$|\arg(\tilde{\lambda}_0) - \arg(\lambda_0)| \leq \sin^{-1} |\tilde{\lambda}_0 - \lambda_0| \leq |\tilde{\lambda}_0 - \lambda_0| + \frac{|\tilde{\lambda}_0 - \lambda_0|^3}{2}, \quad (51)$$

leading to an asymptotic error bound on the ground state energy,

$$\delta E_0 = \frac{|\arg(\tilde{\lambda}_0) - \arg(\lambda_0)|}{\Delta\tau}, \quad (52)$$

$$\leq \frac{2^{3/2}\alpha^{1/2}}{\delta \Delta\tau} [Ke^{-\beta_1 K} + \sin(\Theta_1/2) \cos^2(\Theta_0/4) Ke^{-\beta_2 K}] + \text{h.o.t}, \quad (53)$$

which holds for an arbitrary initial state $|\Phi_0\rangle$. We remark that the error in the excited state energies can be derived in a similar manner. However, the proof requires careful selection of different index sets Ω (since we want to control $|\partial_z \mathcal{C}_\Omega(z_\ell)|$ from below in the perturbative analysis).

Our theoretical result above suggests that the DMD approach has the potential of adeptly approximating the ground state energy, provided that we have access to the overlap $\{s_k\}_k$ whose real and imaginary parts are measured separately using a quantum computer. In practice, we can trivially replicate the preceding proof by considering only the real (or imaginary) parts of the overlaps, *e.g.*, $\Re s_k = \sum_{n=0}^{N-1} p_n \cos(kE_n \Delta\tau)$. By Euler's formula $\Re s_k = \sum_{n=0}^{N-1} p_n (\lambda_n^k + \lambda_n^{-k})/2$, we immediately see that,

$$\sum_{\ell=0}^d c_\ell s_{\ell+k} = 0 \implies \sum_{\ell=0}^{2d} \underline{c}_\ell \underline{s}_{\ell+k} = 0, \quad (54)$$

where

$$\sum_{\ell=0}^{2d} \underline{c}_\ell z^\ell = \prod_{\ell=1}^d (z - \lambda_{n_\ell})(z - \lambda_{n_\ell}^*), \quad (55)$$

is an extended characteristic polynomial containing conjugate pairs eigenphases (λ_n, λ_n^*) and $\underline{s}_k = \sum_{n=0}^{2N-1} (p_n/2) \lambda_n^k$ is the extended overlap matrix element with $(p_n, E_n) = (p_{n-N}, -E_{n-N})$ for $N \leq n \leq 2N-1$. Hence given the data matrix $\{\Re s_k\}_k$, taking $d \mapsto 2d$ or $\alpha \mapsto 2\alpha$ also effectively recovers the ground state energy in the large K limit.

Connection to Padé's rational approximation

Next we present how the DMD approach can be heuristically conceptualized under the framework of Padé approximation. [49, 50] Here we return to our simple assumption $\Omega = [d]$ and work with the efficient approximating sequence $\{\tilde{s}_k\}_k$ with $\tilde{s}_k = \sum_{n \in \Omega} p_n \lambda_n^k \approx s_k$ (recall that $|\sum_{n \in \Omega^c} p_n \lambda_n^k| \leq \sum_{n \in \Omega^c} p_n \ll 1$). Let us now consider the Z -transform of $\{\tilde{s}_k\}_{k \in \mathbb{N}}$,

$$\mathcal{Z}[\{\tilde{s}_k\}](z) = \sum_{k=0}^{\infty} \tilde{s}_k z^{-k}, \quad (56)$$

$$= \sum_{n=0}^{d-1} p_n \sum_{k=0}^{\infty} \left(\frac{\lambda_n}{z} \right)^k = \sum_{n=0}^{d-1} p_n \frac{z}{z - \lambda_n}, \quad (57)$$

which converges in the region $\{z \in \mathbb{C} : |z| > \limsup_k |\tilde{s}_k|^{1/k} = 0\}$. The RHS of Eq. 57 consists of a rational function,

$$\sum_{n=0}^{d-1} p_n \frac{z}{z - \lambda_n} = \sum_{n=0}^{d-1} p_n \frac{z \prod_{\ell \neq n \in \Omega} (z - \lambda_\ell)}{\prod_{\ell \in \Omega} (z - \lambda_\ell)} = \frac{\mathcal{B}_\Omega(z)}{\mathcal{C}_\Omega(z)}, \quad (58)$$

where we recognize that $\mathcal{C}_\Omega(z) = \prod_{\ell \in \Omega} (z - \lambda_\ell) = z^d + \sum_{\ell=0}^{d-1} c_\ell z^\ell$ is the characteristic polynomial in Eq. 17 and $\mathcal{B}_\Omega(z) = \sum_{n \in \Omega} p_n z \prod_{\ell \neq n \in \Omega} (z - \lambda_\ell) \approx z^d + \sum_{\ell=1}^{d-1} b_\ell z^\ell$. Associated with these two polynomials is a rational approximation of the power series,

$$\sum_{k=0}^{\infty} \tilde{s}_k z^k = \frac{\mathcal{B}_\Omega(z^{-1})}{\mathcal{C}_\Omega(z^{-1})} \equiv \frac{\mathcal{B}_{\Omega,P}(z)}{\mathcal{C}_{\Omega,P}(z)}, \quad (59)$$

where $\mathcal{B}_{\Omega,P} = z^d \mathcal{B}_\Omega(z^{-1}) \approx 1 + \sum_{\ell=1}^{d-1} b_{d-\ell} z^\ell$ and $\mathcal{C}_{\Omega,P} = z^d \mathcal{C}_\Omega(z^{-1}) = 1 + \sum_{\ell=1}^d c_{d-\ell} z^\ell$ constitute the Padé approximant. In our context, Padé approximation finds the best rational approximation $(\mathcal{B}_\Omega, \mathcal{C}_\Omega)$ from the time-accumulated overlap data,

$$\int_0^\infty \frac{dt}{\Delta\tau} s(t) e^{iEt} \approx \sum_{k=0}^{\infty} \tilde{s}_k (e^{iE\Delta\tau})^k, \quad (60)$$

whose poles contain the target eigenfrequencies $\{\lambda_n^*\}_{n \in \Omega}$ (up to a complex conjugation). Rearranging Eq. (59) above, we have

$$\sum_{k=0}^{\infty} \tilde{s}_k z^k \mathcal{C}_{\Omega,P}(z) = \mathcal{B}_{\Omega,P}(z) \implies \begin{cases} \sum_{\ell=d-k}^d c_\ell \tilde{s}_{\ell+k-d} = b_{d-k}, & k \in [d] \\ \sum_{\ell=0}^d c_\ell \tilde{s}_{\ell+k} = 0, & k \in \mathbb{N} \end{cases}, \quad (61)$$

upon matching z^k terms on the LHS and the RHS order by order. The first set of derived relations reveals an inherent linkage of the monomial coefficients \vec{c} obtained from the characteristic polynomial $\mathcal{C}_\Omega(z)$ to the set of coefficients \vec{b} used in Padé's construction, whereas the second set of relations simply reiterate the linear dynamics modeled in the DMD approach.

Formal Reduction to Matrix Pencil Methods

In this section, we delve deeper into the common framework that unifies different data-driven strategies. We do so by showcasing an isomorphism between DMD and matrix pencil approaches that are extensively used across scientific fields.

To begin with, let us consider the single input single output (SISO) linear time invariant (LTI) dynamical system,

$$\begin{cases} |\phi_{k+1}\rangle = \mathcal{A}|\phi_k\rangle + \mathcal{B}u_k \\ y_k = \mathcal{C}|\phi_k\rangle + \mathcal{D}u_k \end{cases}, \quad (62)$$

where the system matrices $\mathcal{A} \in \mathbb{C}^{N \times N}$, $\mathcal{B} \in \mathbb{C}^{N \times 1}$, $\mathcal{C} \in \mathbb{C}^{1 \times N}$, and $\mathcal{D} \in \mathbb{C}$. We call N the dimension (order) of the system, $|\phi_k\rangle \in \mathbb{C}^N$ the state vector, $u_k \in \mathbb{C}$ the input, and $y_k \in \mathbb{C}$ the output. Next, the Hamiltonian evolution of a quantum state $|\phi_0\rangle$ can be regarded as the linear dynamical system Eq. (62) with $\mathcal{A} := e^{-iH\Delta\tau}$, $\mathcal{C} := \langle\phi_0|$, and $u_k \equiv 0$, *i.e.*,

$$\begin{cases} |\phi_{k+1}\rangle = \mathcal{A}|\phi_k\rangle \\ y_k = \langle\phi_0|\phi_k\rangle \end{cases}, \quad (63)$$

where $|\phi_k\rangle = e^{-iHk\Delta\tau}|\phi_0\rangle$ is the evolved quantum state after k discrete timesteps. Remark that the system dynamics are determined by the frequencies $\{\lambda_n = e^{-iE_n\Delta\tau}\}_{n=0}^{N-1}$ and the system output yields our overlap observations, *i.e.*, $y_k = s_k$, where the samples s_k given in Eq. (16).

Observe that the (shifted) Hankel matrices $\mathbf{X}, \mathbf{X}' \in \mathbb{C}^{d \times (K+1)}$ associated with the linear dynamical system Eq. (63) can be decomposed as follows,

$$\mathbf{X} = \begin{bmatrix} s_0 & s_1 & \cdots & s_K \\ s_1 & s_2 & \cdots & s_{K+1} \\ \vdots & \vdots & \ddots & \vdots \\ s_{d-1} & s_d & \cdots & s_{K+d-1} \end{bmatrix} = \begin{bmatrix} \mathcal{C} \\ \mathcal{C}\mathcal{A} \\ \vdots \\ \mathcal{C}\mathcal{A}^{d-1} \end{bmatrix} \begin{bmatrix} \mathcal{C}^* & \mathcal{A}\mathcal{C}^* & \cdots & \mathcal{A}^K\mathcal{C}^* \end{bmatrix}, \quad (64)$$

and

$$\mathbf{X}' = \begin{bmatrix} s_1 & s_2 & \cdots & s_{K+1} \\ s_2 & s_3 & \cdots & s_{K+2} \\ \vdots & \vdots & \ddots & \vdots \\ s_d & s_{d+1} & \cdots & s_{K+d} \end{bmatrix} = \begin{bmatrix} \mathcal{C} \\ \mathcal{C}\mathcal{A} \\ \vdots \\ \mathcal{C}\mathcal{A}^{d-1} \end{bmatrix} \mathcal{A} \begin{bmatrix} \mathcal{C}^* & \mathcal{A}\mathcal{C}^* & \cdots & \mathcal{A}^K\mathcal{C}^* \end{bmatrix}. \quad (65)$$

For $d = K + 1 = N$, the frequencies $\{\lambda_n\}_{n=0}^{N-1}$ belong to the spectrum of the linear matrix pencil $(\mathbf{X}', \mathbf{X})$,

$$\mathbf{X}' - \lambda_n \mathbf{X} = \begin{bmatrix} \mathcal{C} \\ \mathcal{C}\mathcal{A} \\ \vdots \\ \mathcal{C}\mathcal{A}^{d-1} \end{bmatrix} (\mathcal{A} - \lambda_n I) \begin{bmatrix} \mathcal{C}^* & \mathcal{A}\mathcal{C}^* & \cdots & \mathcal{A}^K\mathcal{C}^* \end{bmatrix} \implies \det(\mathbf{X}' - \lambda_n \mathbf{X}) = 0, \quad (66)$$

where λ_n solves the corresponding generalized eigenvalue problem $\mathbf{X}'\vec{v}_R = \lambda_n \mathbf{X}\vec{v}_R$ or equivalently $\vec{v}_L\mathbf{X}' = \lambda_n \vec{v}_L\mathbf{X}$ for some right and left eigenvector \vec{v}_R and \vec{v}_L . Note that the latter is identical to the standard eigenvalue problem $\vec{v}_L(\mathbf{X}'\mathbf{X}^+) = z_n \vec{v}_L$ where \mathbf{X}^+ gives the Moore–Penrose pseudo-inverse of our data matrix. Now recall that the DMD system matrix solves the least-square problem,

$$A = \underset{\mathbf{A}_{\text{trial}} \in \mathbb{C}^{d \times d}}{\arg \min} \|\mathbf{X}' - \mathbf{A}_{\text{trial}}\mathbf{X}\|_F^2 \equiv \underset{\vec{a}_{\text{trial}} \in \mathbb{C}^d}{\arg \min} \|(\mathbf{X}')^\top \vec{e}_d - \mathbf{X}^\top \vec{a}_{\text{trial}}\|_2^2, \quad (67)$$

where $\vec{e}_d = (0, \dots, 0, 1)$ labels the d^{th} canonical basis vector in \mathbb{C}^d . The formal solution to Eq. (67) involves computation of the same pseudo-inverse, *i.e.*, $A = \mathbf{X}'\mathbf{X}^+$. In this straightforward case, the amount of data we collect is double the count of target frequency modes ($d + K + 1 = 2N$). As a consequence, the eigenvalues $\{\tilde{\lambda}_n\}_{n=0}^{N-1}$ of the DMD system matrix A should indeed match the eigenvalues $\{\lambda_n\}_{n=0}^{N-1}$ of the exact system matrix \mathcal{A} .

We now move on to the more general case $d \neq K+1 \neq N$. To elucidate the direct correspondence between DMD and different matrix pencil methods used for solving Eq. (66), we first consider factorizing the data matrix \mathbf{X} via the singular value decomposition (SVD), *i.e.*, $\mathbf{X} = U\Sigma V^*$, where $U \in \mathbb{C}^{d \times r}$ and $V \in \mathbb{C}^{(K+1) \times r}$ contain the orthonormal singular vectors and $\Sigma \in \mathbb{R}^{r \times r}$ contains the positive singular values $(\Sigma_{ii})_{1 \leq i \leq r \leq \min(d, K+1)}$ of \mathbf{X} . Assuming a full rank of $r = \min(d, K+1)$, we observe that

$$A = \mathbf{X}'\mathbf{X}^+ = \mathbf{X}'V\Sigma^{-1}U^*, \quad (68)$$

$$\cong U^*(\mathbf{X}'V\Sigma^{-1}U^*)U = U^*\mathbf{X}'V\Sigma^{-1}, \quad (69)$$

$$\cong (\Sigma^{1/2})^{-1}(U^*\mathbf{X}'V\Sigma^{-1})\Sigma^{1/2} = \Sigma^{-1/2}U^*\mathbf{X}'V\Sigma^{-1/2}, \quad (70)$$

where \cong denotes a spectral congruence that preserves the eigenvalues as any similarity transform leaves the spectrum invariant. The formulation of an eigenvalue problem with respect to the RHS of Eq. (70) is known as the eigensystem realization (ERA) method [23–25, 58, 59] for system identification, which manifests a clear equivalence to the DMD approach.

Next we consider simultaneous factorization of the data and shifted data matrix \mathbf{X} and \mathbf{X}' based on SVD of the base Hankel matrix $(s_{i+j})_{0 \leq i \leq d-1, 0 \leq j \leq K+1}$,

$$(s_{i+j})_{ij} = \begin{bmatrix} \underbrace{\mathbf{X}_1}_{d \times 1} & \underbrace{\mathbf{X}_2}_{d \times K} & \underbrace{\mathbf{X}_2}_{d \times 1} \end{bmatrix} = U_{\text{base}}\Sigma_{\text{base}} \begin{bmatrix} V_1 \\ V_2 \\ V_3 \end{bmatrix}^*, \quad (71)$$

for which $\mathbf{X} = [\mathbf{X}_1 \ \mathbf{X}_2]$, $\mathbf{X}' = [\mathbf{X}_2 \ \mathbf{X}_3]$, and Σ_{base} constitutes three singular value blocks consistent with the partition. Since $\mathbf{X} = U_{\text{base}}\Sigma_{\text{base}}[V_1^* \ V_2^*] = U_{\text{base}}\Sigma_{\text{base}}V_{\mathbf{X}}^*$ and $\mathbf{X}' = U_{\text{base}}\Sigma_{\text{base}}[V_2^* \ V_3^*] = U_{\text{base}}\Sigma_{\text{base}}V_{\mathbf{X}'}^*$,

$$A = U_{\text{base}}\Sigma_{\text{base}}V_{\mathbf{X}'}^*(V_{\mathbf{X}}^*)^+\Sigma_{\text{base}}^{-1}U_{\text{base}}^* \cong [V_{\mathbf{X}}^*(V_{\mathbf{X}'}^*)^+]^\top, \quad (72)$$

$$= [(V_{\mathbf{X}'}^*)^\top]^+(V_{\mathbf{X}}^*)^\top, \quad (73)$$

where the congruence follows from invariance of the spectrum under matrix transpose. This SVD-based formulation of the eigenvalue problem associated with the RHS of Eq. (73) is well known as the ESPRIT method [20–22] for signal recovery.

Following our derivation above, let us consider simultaneous factorization of the shifted matrices \mathbf{X} and \mathbf{X}' via the pivoted QR decomposition,

$$(s_{i+j})_{ij} = [\mathbf{X}_1 \ \mathbf{X}_2 \ \mathbf{X}_3] = QR \begin{bmatrix} \Pi_1 \\ \Pi_2 \\ \Pi_3 \end{bmatrix}^\top, \quad (74)$$

where $Q \in \mathbb{C}^{d \times \min(d, K+2)}$ contains orthonormal vectors, $R \in \mathbb{C}^{\min(d, K+2) \times (K+2)}$ is upper triangular, and Π gives a permutation that arranges the diagonals of R in descending (non-increasing) magnitudes. Writing $\mathbf{X} = QR \begin{bmatrix} \Pi_1^\top & \Pi_2^\top \end{bmatrix} = QR\Pi_{\mathbf{X}}^\top$ and $\mathbf{X}' = QR \begin{bmatrix} \Pi_2^\top & \Pi_3^\top \end{bmatrix} = QR\Pi_{\mathbf{X}'}^\top$, we have

$$A = QR\Pi_{\mathbf{X}'}^\top(R\Pi_{\mathbf{X}}^\top)^+Q^* \cong \left[R_{\text{diag}}^{-1}(R\Pi_{\mathbf{X}}^\top)(R\Pi_{\mathbf{X}}^\top)^+R_{\text{diag}} \right]^\top, \quad (75)$$

$$= \left[(R_{\text{diag}}^{-1}R\Pi_{\mathbf{X}}^\top)^+ \right]^\top (R_{\text{diag}}^{-1}R\Pi_{\mathbf{X}}^\top)^\top, \quad (76)$$

$$= \left[(R_{\text{diag}}^{-1}R\Pi_{\mathbf{X}}^\top)^\top \right]^+ (R_{\text{diag}}^{-1}R\Pi_{\mathbf{X}}^\top)^\top, \quad (77)$$

where R_{diag} denotes the diagonal part of R . The QR-based matrix pencil method precisely refers to the formulation of eigenvalue problem associated with the RHS of Eq. (77). Therefore the DMD approach for full-rank problems is algorithmically isomorphic to these various data-informed methods developed in scientific and engineering communities, and meanwhile it remains full compactness without the need of additional square root or pseudo-inverse computation.

Ground State Energy Estimation of Molecular Hamiltonians

Here we provide additional data and details for the range of molecular Hamiltonians considered in this study. For Cr_2 dimer (both here and in the main text), we work with the def2-SVP basis set [60] (bond length 1.5 Å, 30 orbitals, and 24 electrons). We restrict our simulation to the widely studied 30 orbital active space and truncate the Hilbert space, considering only a subset of Slater determinants that we choose using ASCI [51, 52]. All data shown in the main text and here are a truncation of size 4000, selected from a one million determinant ASCI calculation where the 4000 determinants with the largest coefficients are included. In addition to Cr_2 , we include LiH (3-21g basis set [61], bond length 1.5 Å, 11 orbitals, and 4 electrons) and H_6 chain (STO-6g basis set [62], bond length 1.5 Å, 6 orbitals, and 6 electrons).

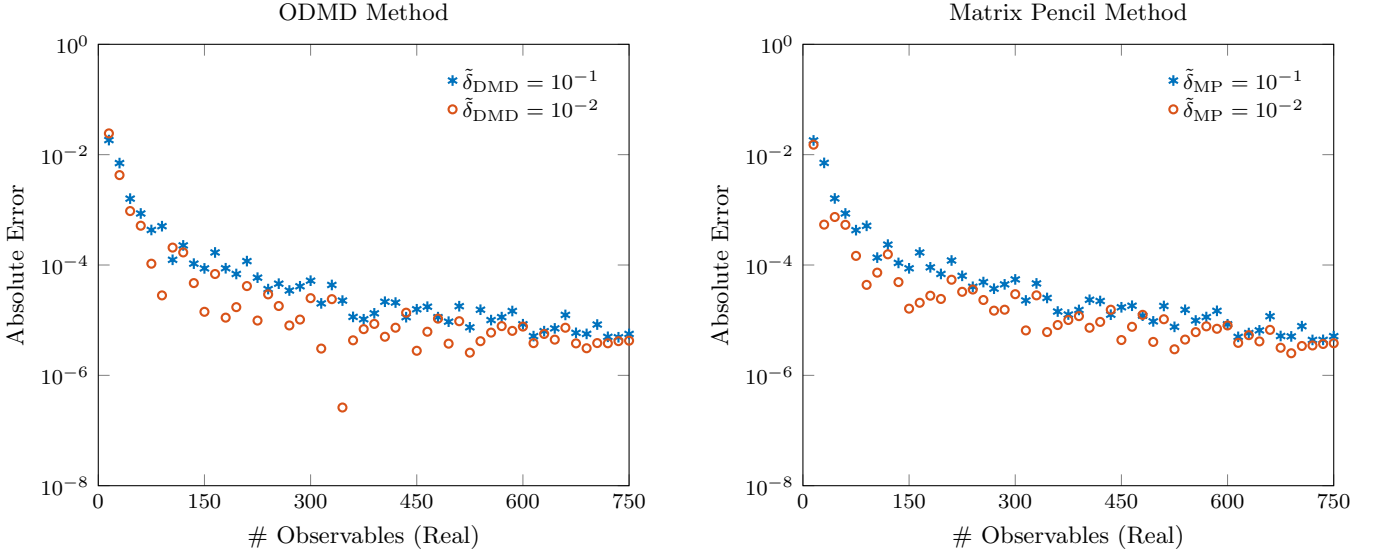


FIG. 6. Data comparing ODMD and the matrix pencil method with different singular value truncations ($\tilde{\delta}_{\text{DMD}}$ and $\tilde{\delta}_{\text{MP}}$) for Cr_2 with noise level $\epsilon = 10^{-3}$. A timestep of $\Delta t = 3$ is used for generating the results.

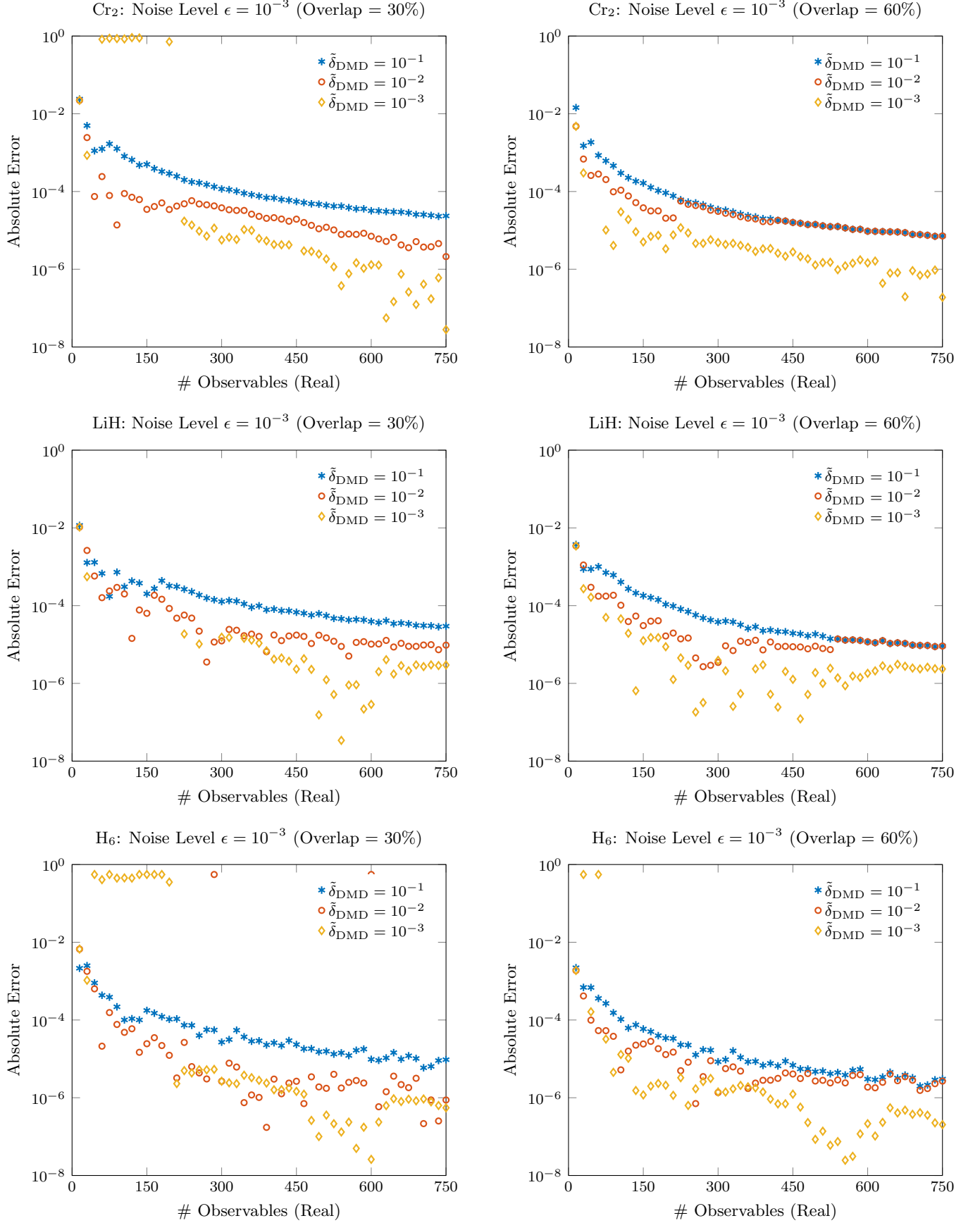


FIG. 7. Comparison of ODMD ground state energy convergence for a range of molecules with varying reference-ground state overlap probabilities p_0 and singular value truncations $\tilde{\delta}_{\text{DMD}}$. A timestep of $\Delta t = 3$ is used for generating the results.